# Multiple prebiotic metals mediate translation

Marcus S. Bray[a,1], Timothy K. Lenz[b,1], Jay William Haynes[b], Jessica C. Bowman[b], Anton S. Petrov[b], Amit R. Reddi[b], Nicholas V. Hud[b], Loren Dean Williams[b,2], and Jennifer B. Glass[c,2]

[a]School of Biological Sciences, Georgia Institute of Technology, Atlanta, GA 30332; [b]School of Chemistry and Biochemistry, Georgia Institute of Technology, Atlanta, GA 30332; and [c]School of Earth and Atmospheric Sciences, Georgia Institute of Technology, Atlanta, GA 30332

Edited by Ada Yonath, Weizmann Institute of Science, Rehovot, Israel, and approved October 19, 2018 (received for review March 5, 2018)

**Today, $Mg^{2+}$ is an essential cofactor with diverse structural and functional roles in life's oldest macromolecular machine, the translation system. We tested whether ancient Earth conditions (low $O_2$, high $Fe^{2+}$, and high $Mn^{2+}$) can revert the ribosome to a functional ancestral state. First, SHAPE (selective 2′-hydroxyl acylation analyzed by primer extension) was used to compare the effect of $Mg^{2+}$, $Fe^{2+}$, and $Mn^{2+}$ on the tertiary structure of rRNA. Then, we used in vitro translation reactions to test whether $Fe^{2+}$ or $Mn^{2+}$ could mediate protein production, and quantified ribosomal metal content. We found that (*i*) $Mg^{2+}$, $Fe^{2+}$, and $Mn^{2+}$ had strikingly similar effects on rRNA folding; (*ii*) $Fe^{2+}$ and $Mn^{2+}$ can replace $Mg^{2+}$ as the dominant divalent cation during translation of mRNA to functional protein; and (*iii*) Fe and Mn associate extensively with the ribosome. Given that the translation system originated and matured when $Fe^{2+}$ and $Mn^{2+}$ were abundant, these findings suggest that $Fe^{2+}$ and $Mn^{2+}$ played a role in early ribosomal evolution.**

translation | ribosome | iron | manganese | magnesium

Life arose around 4 billion years ago on an anoxic Earth with abundant soluble $Fe^{2+}$ and $Mn^{2+}$ (1–5). Biochemistry had access to vast quantities of these metals for over a billion years before biological $O_2$ production was sufficient to oxidize and precipitate them. The pervasive use of these "prebiotic" metals in extant biochemistry, despite current barriers to their biological acquisition, likely stems from their importance in the evolution of the early biochemical systems.

The translation system, which synthesizes all coded protein (6, 7), originated and matured during the Archean Eon (4 Ga to 2.5 Ga) in low-$O_2$, high-$Fe^{2+}$, and high-$Mn^{2+}$ conditions (8). The common core of the ribosome, and many other aspects of the translation system, has remained essentially frozen since the last universal common ancestor (9). In extant biochemistry, $Mg^{2+}$ ions are essential for both structure and function of the ribosome (10) and other enzymes involved in translation (11). In ribosomes, $Mg^{2+}$ ions engage in a variety of structural roles (Table 1), including in $Mg^{2+}$-rRNA clamps (12, 13) (Fig. 1*A*), in dinuclear microclusters that frame the peptidyl transferase center (PTC) (13) (Fig. 1*B*), and at the small subunit–large subunit (SSU–LSU) interface (14) (Fig. 1*C*). Functional $Mg^{2+}$ ions stabilize a critical bend in mRNA between the P-site and A-site codons (15) (Fig. 1*D*), and mediate rRNA–tRNA and rRNA–mRNA interactions (16) (Fig. 1 *E* and *F*). $Mg^{2+}$ ions also interact with some rProteins (17). Additionally, accessory enzymes needed for translation—aminoacyl-tRNA synthetases, methionyl-tRNA transformylase, creatine kinase, myokinase, and nucleoside diphosphate kinase—require $Mg^{2+}$ ions as cofactors (Table 1).

Multiple types of cationic species can interact productively with RNAs in a variety of systems (18–20). Recent results support a model in which $Fe^{2+}$ and $Mn^{2+}$, along with $Mg^{2+}$, were critical cofactors in ancient nucleic acid function (21). As predicted by this model, functional $Mg^{2+}$-to-$Fe^{2+}$ substitutions under anoxic conditions were experimentally verified to support RNA folding and catalysis by ribozymes (22, 23), a DNA polymerase, a DNA ligase, and an RNA polymerase (24). Functional $Mg^{2+}$-to-$Mn^{2+}$ substitution has long been known for DNA polymerases (24–26). For at least some nucleic acid-processing enzymes, optimal activity is observed at lower concentrations of $Fe^{2+}$ than $Mg^{2+}$ (22, 24). Based on these previous results, we hypothesized that $Fe^{2+}$ and $Mn^{2+}$ could partially or fully replace $Mg^{2+}$ during translation. In this study, we relocated the translation system to the low-$O_2$, $Fe^{2+}$-rich, or $Mn^{2+}$-rich environment of its ancient roots, and compared its structure, function, and cation content under modern vs. ancient conditions.

## Results

**$Fe^{2+}$ and $Mn^{2+}$ Fold LSU rRNA to a Near-Native State.** To test whether $Fe^{2+}$ or $Mn^{2+}$ can substitute for $Mg^{2+}$ in folding rRNA to a native-like state, we compared folding of LSU rRNA of the bacterial ribosome in the presence of $Mg^{2+}$, $Fe^{2+}$, or $Mn^{2+}$ by SHAPE (selective 2′-hydroxyl acylation analyzed by primer extension). SHAPE provides quantitative, nucleotide-resolution information about RNA flexibility, base pairing, and 3D structure, and has previously been used to monitor the influence of cations, small molecules, or proteins on RNA structure (27–32). We previously used SHAPE to show that the LSU rRNA adopts a near-native state in the presence of $Mg^{2+}$, with the core interdomain architecture of the assembled ribosome and residues positioned for interactions with rProteins (33). Here, SHAPE experiments were performed in an anoxic chamber to maintain the oxidation state of the metals and to prevent Fenton cleavage. The minimum concentration required to fully fold

## Significance

Ribosomes are found in every living organism, where they are responsible for the translation of messenger RNA into protein. The ribosome's centrality to cell function is underscored by its evolutionary conservation; the core structure has changed little since its inception ∼4 billion years ago when ecosystems were anoxic and metal-rich. The ribosome is a model system for the study of bioinorganic chemistry, owing to the many highly coordinated divalent metal cations that are essential to its function. We studied the structure, function, and cation content of the ribosome under early Earth conditions (low $O_2$, high $Fe^{2+}$, and high $Mn^{2+}$). Our results expand the roles of $Fe^{2+}$ and $Mn^{2+}$ in ancient and extant biochemistry as cofactors for ribosomal structure and function.

Author contributions: M.S.B., J.C.B., A.R.R., N.V.H., L.D.W., and J.B.G. designed research; M.S.B., T.K.L., and J.W.H. performed research; A.S.P., A.R.R., and N.V.H. contributed new reagents/analytic tools; M.S.B., T.K.L., J.W.H., J.C.B., A.S.P., L.D.W., and J.B.G. analyzed data; and M.S.B., L.D.W., and J.B.G. wrote the paper.

The authors declare no conflict of interest.

This article is a PNAS Direct Submission.



[1]M.S.B. and T.K.L. contributed equally to this work.

[2]To whom correspondence may be addressed. Email: loren.williams@chemistry.gatech.edu or jennifer.glass@eas.gatech.edu.

This article contains supporting information online at www.pnas.org/lookup/suppl/doi:10.1073/pnas.1803636115/-/DCSupplemental.

**Table 1. Structural and functional roles for select divalent cations ($M^{2+}$) in the translation system**

| Translation system component(s) | Location of divalent ion | Role of divalent cation | Optimal [$Mg^{2+}$], mM |
|---|---|---|---|
| Ribosome | | | |
| LSU/SSU | $M^{2+}$-rRNA clamps (12) | Mediates and maintains folding/structure of rRNAs | ~10 (34) |
| LSU | Dinuclear microclusters (13) | Frames PTC | ~10 (34) |
| LSU/SSU | LSU/SSU interface (27) | Mediates docking of mRNA to SSU and association of SSU with LSU | ~10 (34) |
| SSU/mRNA | Critical bend in mRNA between the P-site and A-site codons (16, 55) | Maintains correct reading frame on mRNA | ~10 (34) |
| A-site tRNA/P-site tRNA | tRNA-tRNA interface (27) | Stabilize tRNAs in the PTC | ~10 (34) |
| LSU/tRNA | rRNA-tRNA interface (27) | Stabilize rRNA-tRNA in the PTC | ~10 (34) |
| Auxiliary | | | |
| EF-Tu | GTP binding site (56) | Stabilizes the transition state | 5 to 15 (57) |
| EF-G | GTP binding site (58) | Stabilizes the transition state | n.a. |
| Aminoacyl-tRNA synthetases | ATP binding site (59) | Stabilizes the transition state | >1 (60) |
| Methionyl-tRNA transformylase | ATP binding site (61) | Stabilizes the transition state | 7 (61) |
| Creatine kinase | NTP binding site (62) | Stabilizes the transition state | ~5 (62) |
| Myokinase | Acceptor NDP binding site (63) | Stabilizes the transition state | ~3 (45) |
| Nucleoside diphosphate kinase | NTP binding site (64) | Stabilizes the transition state | >1 (64) |
| Pyrophosphatase | Active site (65) | Stabilizes the transition state | >7 (66) |

All biomolecules in the table have been shown to require $Mg^{2+}$ and may also be active with $Fe^{2+}$ or $Mn^{2+}$; "n.a." indicates that data are not available.

rRNA (10 mM $Mg^{2+}$, 2.5 mM $Fe^{2+}$, or 2.5 mM $Mn^{2+}$) was used for all SHAPE experiments (Datasets S1 and S2).

Addition of $Mg^{2+}$, $Fe^{2+}$, or $Mn^{2+}$ induced widespread structural changes in the LSU rRNA in the presence of $Na^{+}$, as reflected in SHAPE profiles (see *Materials and Methods*) and displayed as "heat maps" on the LSU rRNA secondary structure (Fig. 2 and *SI Appendix*, Fig. S1). Among the nucleotides forming the PTC, similar SHAPE profiles were obtained in the presence of $Mg^{2+}$, $Fe^{2+}$, or $Mn^{2+}$ (*SI Appendix*, Fig. S1). The $\Delta Fe^{2+}$ and $\Delta Mg^{2+}$ heat maps obtained for the entire 23S rRNA are nearly identical in most regions (Fig. 2 *D* and *E*). As expected for conversion of secondary structure to fully folded tertiary structure, helices tended to be invariant, whereas loops and bulges were impacted by addition of $Mg^{2+}$, $Fe^{2+}$, or $Mn^{2+}$. For the 23S rRNA, 86% of nucleotides (43/50) that exhibited a significant response (>0.3 SHAPE units) to $Mg^{2+}$ also exhibited a similar trend with $Fe^{2+}$. The greatest discrepancy between $Fe^{2+}$ and $Mg^{2+}$ was observed in the L11 binding domain (Fig. 2 *D* and *E*).

**$Fe^{2+}$ and $Mn^{2+}$ Mediate Translation.** Translation reactions were performed in an anoxic chamber in the presence of various cations and cation concentrations. Production of the protein dihydrofolate reductase (DHFR) from its mRNA was used to monitor translational activity. Protein synthesis was assayed by measuring the rate of NADPH oxidation by DHFR. These reactions were conducted in a small background of 2.5 mM $Mg^{2+}$ (*SI Appendix*, Fig. S2*A*). This background is below the requirement to support translation, consistent with previous findings that a minimum of ~5 mM $Mg^{2+}$ is needed for assembly of mRNA onto the SSU (34, 35). As a control, we recapitulated the previously established $Mg^{2+}$ dependence of the translation system, and then repeated the assay with $Fe^{2+}$.

Activity of the translation system with variation in [$Fe^{2+}$] closely tracks activity with variation in [$Mg^{2+}$] (Fig. 3). Below 7.5 mM, total divalent cation concentration, minimal translation occurred with either $Fe^{2+}$ or $Mg^{2+}$, as expected (36). Activity peaked at 9.5 mM for both cations and decreased modestly beyond the optimum. At a given divalent cation concentration, $Fe^{2+}$ supported around 50 to 80% of activity with $Mg^{2+}$ (Fig. 4). This result was observed with translation reactions run for 15, 30, 45, 60, 90, and 120 min at the optimal divalent cation concentrations. $Mn^{2+}$ also supported similar translation activity to $Fe^{2+}$ at optimal divalent concentrations (*SI Appendix*, Fig. S3). Along with $Mg^{2+}$, $Fe^{2+}$, and $Mn^{2+}$, we investigated whether other divalent cations could support translation. No translation activity was detected with $Co^{2+}$, $Cu^{2+}$, or $Zn^{2+}$ (*SI Appendix*, Fig. S3).

To test whether alternative divalent cations could completely replace $Mg^{2+}$ in translation, we decreased the background $Mg^{2+}$ from 2.5 mM to 1 mM by thoroughly washing the ribosomes before translation reactions with 7 mM to 11 mM $Fe^{2+}$ or $Mn^{2+}$ (*SI Appendix*, Fig. S2*B*). With 1 mM background $Mg^{2+}$, $Fe^{2+}$ supported 12 to 23% of the activity with $Mg^{2+}$ over the concentrations tested, while $Mn^{2+}$ supported 43 to 50% activity relative to $Mg^{2+}$ (Fig. 5*A*). Washing the factor mix allowed us to decrease the background $Mg^{2+}$ in translation reactions to ~4 μM to 6 μM (*SI Appendix*, Fig. S2*C*). At this level, minimal protein production was observed with $Fe^{2+}$, while $Mn^{2+}$ supported 29 to 38% of the activity measured with $Mg^{2+}$ (Fig. 5*B*).

**Fe and Mn Associate Extensively with the Ribosome.** To experimentally confirm that Fe and Mn associate with the assembled ribosome, we analyzed the total Fe or Mn content of ribosomes after incubation in anoxic reaction buffer containing 7 mM $Fe^{2+}$ or 7 mM $Mn^{2+}$. Under the conditions of our translation reactions, 584 ± 9 Fe atoms or 507 ± 28 Mn atoms associate with each ribosome.

Finally, we computationally investigated whether $Mg^{2+}$, $Fe^{2+}$, and $Mn^{2+}$ might be interchangeable during translation, using quantum mechanical characterization of $M^{2+}$-rRNA clamps (Fig. 1*A* and *SI Appendix*, Fig. S4), which are abundant in the ribosome (12, 13). The geometries of $Mg^{2+}$-rRNA, $Fe^{2+}$-rRNA, and $Mn^{2+}$-rRNA clamps are nearly identical (*SI Appendix*, Table S1). However, due to the accessibility of their d orbitals, more charge is transferred to $Fe^{2+}$ or $Mn^{2+}$ than to $Mg^{2+}$ (*SI Appendix*, Table S2). The effect of the modestly greater radius of $Mn^{2+}$ (*SI Appendix*, Table S1) is offset by d-orbital charge transfer (*SI Appendix*, Table S2), leading to elevated stability of the $Fe^{2+}$-rRNA clamp over the $Mn^{2+}$-rRNA clamp (*SI Appendix*, Table S3).

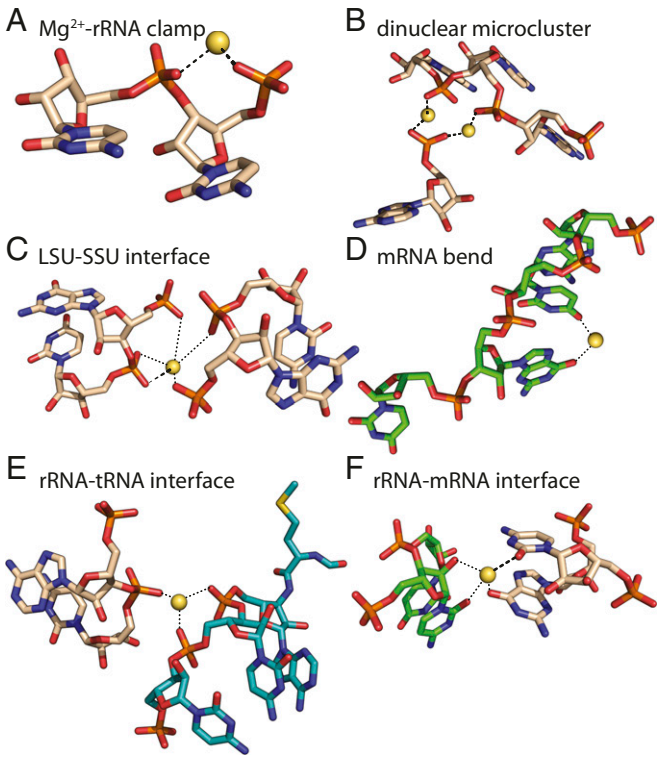


**Fig. 1.** Divalent cations serve many structural and functional roles in the ribosome. $Mg^{2+}$ ions (*A*) form bidentate clamps with adjacent phosphate groups of rRNA, (*B*) form dinuclear microclusters that frame the rRNA of the PTC, (*C*) stabilize the LSU–SSU interface, (*D*) stabilize a functional kink in mRNA, (*E*) stabilize association of tRNA (teal) with 23S rRNA (beige carbon atoms), and (*F*) stabilize association of mRNA (green) with 16S rRNA (beige carbon atoms). Thick dashed lines are first-shell RNA interactions of $Mg^{2+}$. Dotted lines indicate second-shell interactions. Images are of the *T. thermophilus* ribosome (PDB ID code 1VY4). This figure was generated with the program RiboVision (54).

## Discussion

In this study, we successfully replaced ribosomal $Mg^{2+}$ with $Fe^{2+}$ or $Mn^{2+}$ under conditions mimicking the anoxic Archean Earth. Previously, the only divalent cation known to mediate rRNA folding and function was $Mg^{2+}$. We found that isolated rRNA folds to essentially the same global state (37, 38) with $Mg^{2+}$, $Fe^{2+}$, or $Mn^{2+}$ under anoxia. This study revealed that $Fe^{2+}$ or $Mn^{2+}$ can serve as the dominant divalent cation during translation. $Mg^{2+}$ at 2.5 mM was insufficient to mediate protein synthesis; 5 mM additional $Mg^{2+}$, $Fe^{2+}$, or $Mn^{2+}$ restored translational activity. These findings suggest that functional substitutions of $Mn^{2+}$ or $Fe^{2+}$ for $Mg^{2+}$ can occur in large ribozymes, similar to previous reports for protein enzymes and small ribozymes (24–26, 39, 40). Near-complete removal of $Mg^{2+}$ prevented $Fe^{2+}$-mediated translation and partially inhibited $Mn^{2+}$-mediated translation, suggesting that $Mg^{2+}$ is optimal for some specific roles in the translation system. Regardless, the general effectiveness of $Mn^{2+}$ or $Fe^{2+}$ for $Mg^{2+}$ substitutions in the translation system is astounding considering the enormous number of divalent cations associated with a given ribosome, and the broad scope of their structural and functional roles (10, 11) (Fig. 1 and Table 1).

The observation that >500 Fe or Mn ions can associate with a bacterial ribosome is consistent with the number of $Mg^{2+}$ ions observed by X-ray diffraction [100 to 1,000 $Mg^{2+}$ per ribosome (41)], and supports a model in which $Fe^{2+}$ or $Mn^{2+}$ has replaced $Mg^{2+}$ as the dominant divalent cation in our experiments. The high capacity of ribosomes for $Fe^{2+}$ and $Mn^{2+}$ reflects all rRNA-associated divalent cations, including condensed, glassy, and chelated divalent cations (42), and, in addition, we presume that $Fe^{2+}$ or $Mn^{2+}$ can associate with a variety of rProteins, including those previously shown to bind $Zn^{2+}$ (e.g., uS2, uS15, bS16, uS17, uL2, uL13, bL31, and bL36 in *Escherichia coli*) (43).

The differences in protein production observed among the three divalent cations likely arise from a variety of evolutionary and physiological factors. For instance, *E. coli* ribosomes may be evolutionarily adapted to $Mg^{2+}$ instead of $Fe^{2+}$ or $Mn^{2+}$. The difference in translational activity between $Mn^{2+}$ and $Fe^{2+}$, particularly when background $Mg^{2+}$ was removed, suggests that $Mn^{2+}$ is more viable than $Fe^{2+}$ upon full substitution. $Mn^{2+}/Mg^{2+}$ interchangeability may depend on relative stabilities of $Mn^{2+}$ and $Mg^{2+}$ in $M^{2+}$-rRNA clamps (*SI Appendix*, Fig. S4). Besides the ribosome, our translation reactions utilize many accessory proteins such as elongation factors and aminoacyl-tRNA synthetases that also have divalent cation requirements. Decreased activity of any of one these systems with $Mn^{2+}$ and $Fe^{2+}$ would cause a pinch point in an otherwise fully functional translation system. Indeed, the relative activity of myokinase and arginine tRNA synthetase are both lower with $Mn^{2+}$ or $Fe^{2+}$ than with $Mg^{2+}$ (44, 45).

While intracellular $Mg^{2+}$ is around $10^{-3}$ M (46), specific physiological or environmental conditions can significantly elevate intracellular $Fe^{2+}$ and $Mn^{2+}$. Under oxidative stress, some microbes accumulate excess $Mn^{2+}$. For example, radiation-tolerant *Deinococcus radiodurans* contains ~10 times higher $Mn^{2+}$ than *E. coli* [$\sim10^{-5}$ M $Mn^{2+}$ (47, 48)]. In the absence of $O_2$, *E. coli* contains ~10 times higher labile $Fe^{2+}$ ($\sim10^{-4}$ M) than in the presence of $O_2$ [$\sim10^{-5}$ M (49)]. Thus, it is possible that the absence of $Fe^{2+}$ and $Mn^{2+}$ in experimentally determined ribosomal structures is reflective of culturing, purification, or crystallization conditions (high $O_2$, high $Mg^{2+}$, low $Fe^{2+}$, and low $Mn^{2+}$), and that other cations may also be present under diverse physiological conditions.

We have shown that the translation system functions with mixtures of divalent cations, which are variable during long-term evolutionary history and during short-term changes in bioavailability and oxidative stress. When combined with previous results that DNA replication and transcription can be facilitated by $Fe^{2+}$ and $Mn^{2+}$ (18–20, 22–26, 39, 40), our findings that both $Fe^{2+}$ and $Mn^{2+}$ can mediate rRNA folding and translation of active protein has revealed that these prebiotic divalent metals can facilitate the entire central dogma of molecular biology (DNA→RNA→protein). These findings raise important questions about evolutionary and physiological roles for $Fe^{2+}$ and $Mn^{2+}$ in ancient and extant biological systems. Were $Mg^{2+}$, $Fe^{2+}$, and $Mn^{2+}$ collaborators as cofactors on the ancient Earth, when $Fe^{2+}$ and $Mn^{2+}$ were more abundant (1–5), and $Mg^{2+}$ was less abundant (2), than today? What was the role of $Fe^{2+}$ and $Mn^{2+}$ in the origin and early evolution of the translational system? Finally, what are the implications for ribosome-bound $Fe^{2+}$ in oxidative damage and disease (50, 51)?

## Materials and Methods

**rRNA Folding via SHAPE.** SHAPE (28, 32, 33) was conducted on the ~2,900-nt *Thermus thermophilus* 23 rRNA (LSU) in 250 mM monovalent cation ($Na^+$ or $K^+$) to favor formation of secondary structure, and in 250 mM $Na^+$ or $K^+$ plus various divalent cations (10 mM $MgCl_2$, 2.5 mM $FeCl_2$, or 2.5 mM $MnCl_2$) to favor tertiary interactions. These divalent cation concentrations are sufficient to fold rRNA. To keep rRNA samples from $O_2$, solutions of rRNA alone or 200 mM NaOAc or KOAc plus 50 mM Na-Hepes (pH 8) or K-Hepes (pH 8) and divalent cations were lyophilized and transferred into an anoxic chamber with a 98% Ar and 2% $H_2$ atmosphere. The rRNA solutions were rehydrated with nuclease-free, degassed water, and added to the dried salts to achieve the appropriate concentrations. After rRNA modification reactions, divalent cations were removed by chelating beads. Samples were removed from the anoxic chamber before reverse transcription and analysis by capillary electrophoresis as in ref. 33. Essentially identical SHAPE profiles were observed with $Na^+$ or $K^+$ alone (*SI Appendix*, Fig. S1), as previously described (32, 52), and for monovalent cations in combination $Mg^{2+}$, $Fe^{2+}$, or

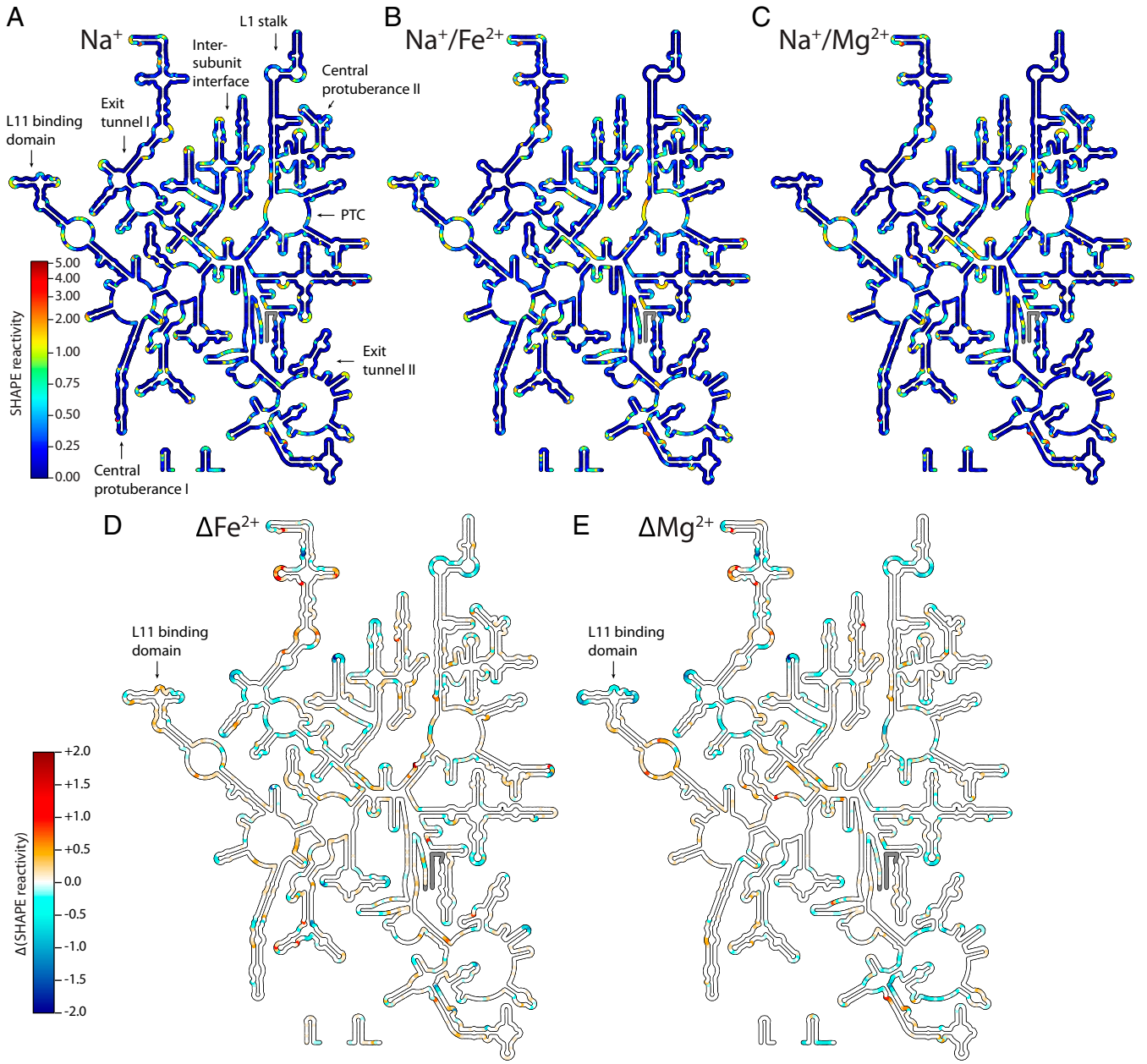


**Fig. 2.** SHAPE reactivities mapped onto the *T. thermophilus* LSU rRNA secondary structure in (*A*) $Na^+$, (*B*) $Na^+/Fe^{2+}$, or (*C*) $Na^+/Mg^{2+}$. Key functional elements are labeled in *A*, and the color scale in *A* applies to *B* and *C*. (*D*) $Fe^{2+}$-induced changes ($\Delta Fe^{2+}$) in SHAPE reactivity calculated by subtracting $Na^+$ data from $Na^+/Fe^{2+}$ data for each nucleotide, and (*E*) $Mg^{2+}$-induced changes ($\Delta Mg^{2+}$) in SHAPE reactivity calculated by subtracting $Na^+$ data from $Na^+/Mg^{2+}$ data for each nucleotide. The color scale shown for *D* also applies to *E*. Positive values indicate increased SHAPE reactivity in presence of the divalent cation, while negative values denote decreased reactivity. Regions where data are not available (5′ and 3′ ends) are gray. These figures were generated with the program RiboVision (54). The L11 binding region, where the greatest discrepancy between $Fe^{2+}$ and $Mg^{2+}$ is observed, is indicated with an arrow.

$Mn^{2+}$ (Fig. 2 and *SI Appendix*, Fig. S1). Nucleotides were classified as exhibiting a significant change in SHAPE reactivity if the difference between the initial reactivity (in $Na^+$) and final reactivity (in $Na^+/Mg^{2+}$, $Na^+/Fe^{2+}$, or $Na/Mn^{2+}$) was >0.3 SHAPE units. To compare the $Mg^{2+}$, $Fe^{2+}$, and $Mn^{2+}$ responsiveness of specific nucleotides, we binned nucleotides into three categories (increased, decreased, or little/no change) based on their general SHAPE reactivity response to each divalent cation (SHAPE data are found in Datasets S1 and S2).

**In Vitro Translation.** Each 30-μL reaction contained 2 μM (4.5 μL of 13.3 μM stock) *E. coli* ribosomes in 10 mM $Mg^{2+}$ (catalog # P0763S; New England Biolabs), 3 μL of factor mix (with RNA polymerase, and transcription/translation factors in 10 mM $Mg^{2+}$) from the PURExpress Δ Ribosome Kit (E3313S; New England Biolabs), 0.1 mM amino acid mix (catalog # L4461; Promega), and 0.2 mM tRNAs from *E. coli* MRE 600 (product # TRNAMRE-RO; Sigma-Aldrich). Thus, a total of 2.5 mM "background" $Mg^{2+}$ was present in each reaction (*SI Appendix*, Fig. S2*A*). To remove the background $Mg^{2+}$, we exchanged the buffer of the ribosome and factor mix using centrifugal filter units. Thirty microliters of either ribosome solution or factor mix was added to an Amicon Ultra 0.5-mL centrifugal filter (Millipore-Sigma), followed by 450 μL of divalent-free buffer (20 mM Hepes pH 7.6, 30 mM KCl, and 7 mM β-mercaptoethanol). Samples were spun at 14,000 × *g* at 4 °C until the minimum sample volume (~15 μL) was reached. The samples were resuspended in 450 μL of divalent-free buffer, and centrifugation was repeated. The samples were then transferred to new tubes, and 15 μL of divalent-free buffer was added to bring the volume to 30 μL. This process decreased $Mg^{2+}$ concentrations in the ribosome and factor mix from 10 mM

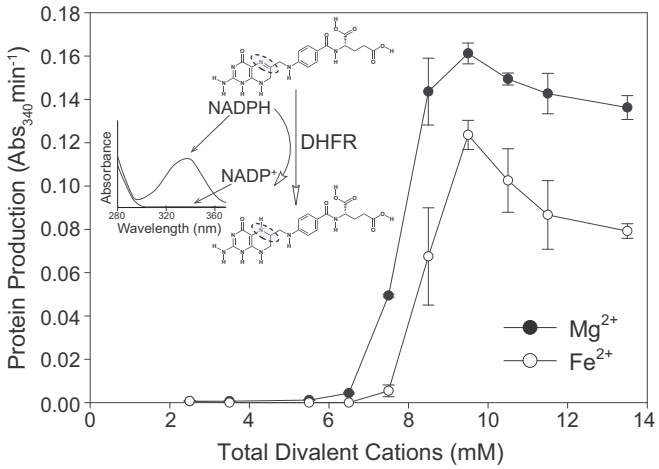


**Fig. 3.** $Mg^{2+}$ and $Fe^{2+}$ stimulate translational activity over a range of concentrations. The activity of the translation product (DHFR, which catalyzes the oxidation of NADPH, with a maximum absorbance at 340 nm) was used as a proxy for protein production. Translation reactions were run for 120 min. All translation reactions contained 2.5 mM background $Mg^{2+}$, to which varying amounts of additional $Mg^{2+}$ or $Fe^{2+}$ were added. The error bars for triplicate experiments ($n$ = 3) are plotted as the SEM. The *Inset* shows the absorbance spectrum and chemical structures of the substrate, NADPH, and product, $NADP^+$. The dashed circles highlight the nitrogen and carbon atoms of dihydrofolic acid that are reduced by DHFR using NADPH.

to 10 μM to 30 μM $Mg^{2+}$, resulting in 4 μM to 6 μM $Mg^{2+}$ in each reaction (*SI Appendix*, Fig. S2 *B* and *C*).

**Translation Experimental Conditions.** All reactions (30 μL total volume) were assembled and incubated in an anoxic chamber. Divalent cation salts [$MgCl_2$, $FeCl_2$, $MnCl_2$, $Zn(OAc)_2$, $CoCl_2$, $CuSO_4$] were added to 7 mM final concentration, with the exception of $MgCl_2$, $FeCl_2$, and $MnCl_2$, which were tested over a range of concentrations (*SI Appendix*, Fig. S2). Solutions were clear, with no indication of metal precipitate, suggesting that reduced, divalent metals cations were the primary chemical species. All experiments were assembled in the following order: DHFR mRNA (~5 μg per 30-μL reaction), factor mix, ribosomes, amino acids, tRNA, nuclease-free $H_2O$, and reaction buffer (see *SI Appendix* for details on mRNA template and reaction buffer recipe). Changing the order of reactant addition did not affect translational activity. Reactions were run in triplicate on a 37 °C heat block for up to 120 min. Reactions were quenched on ice and stored on ice until they were assayed for protein synthesis.

**Protein Activity Assay.** Protein synthesis was measured using a DHFR assay kit (product # CS0340; Sigma-Aldrich), which measures the oxidation of NADPH (60 mM) to $NADP^+$ by dihydrofolic acid (51 μM). Assays were performed by adding 5 μL of protein synthesis reaction to 995 μL of 1× assay buffer. The NADPH absorbance peak at 340 nm ($Abs_{340}$) was measured at 15-s intervals over 2.5 min. The slope of the linear regression of $Abs_{340}$ vs. time was used to determine protein activity ($Abs_{340}$ $min^{-1}$). Different counter ions ($Cl^-$, $CH_3COO^-$, $SO_4^{2-}$) had no effect on protein synthesis from mRNA. To our knowledge, no dependence on, nor inhibitory effect of, $Mg^{2+}$ or $Fe^{2+}$ exists for DHFR. We confirmed this by varying the metal concentrations in our assay reaction, which had no effect on DHFR activity.

**Ribosome Metal Content.** The Fe and Mn content of *E. coli* ribosomes was measured by total reflection X-ray fluorescence spectroscopy after the ribosomes were incubated in 7 mM $FeCl_2$ or 7 mM $MnCl_2$. See *SI Appendix* for additional details.

**Quantum Mechanical Calculations.** The atomic coordinates of a $Mg^{2+}$-rRNA clamp were initially extracted from the X-ray structure of the *Haloarcula marismortui* LSU [Protein Data Bank (PDB) ID code 1JJ2] (53). The free 5′ and 3′ termini of the phosphate groups were capped with methyl groups in lieu

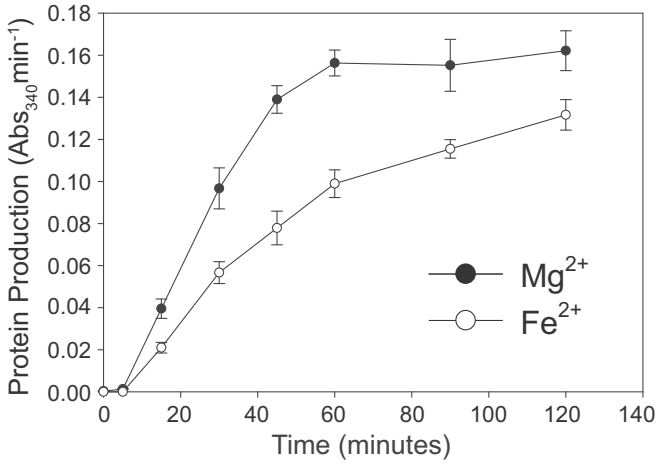


**Fig. 4.** $Fe^{2+}$ consistently supports 50 to 80% of the translational activity as $Mg^{2+}$ when the translation experiments are run for 15 min to 120 min. The activity of the translation product (DHFR, which catalyzes the oxidation of NADPH, with a maximum absorbance at 340 nm) was used as a proxy for protein production. All translation reactions contained 2.5 mM background $Mg^{2+}$, to which 7 mM additional $Mg^{2+}$ or $Fe^{2+}$ were added, totaling 9.5 mM divalent cation. The error bars for triplicate experiments ($n$ = 3) are plotted as the SEM.

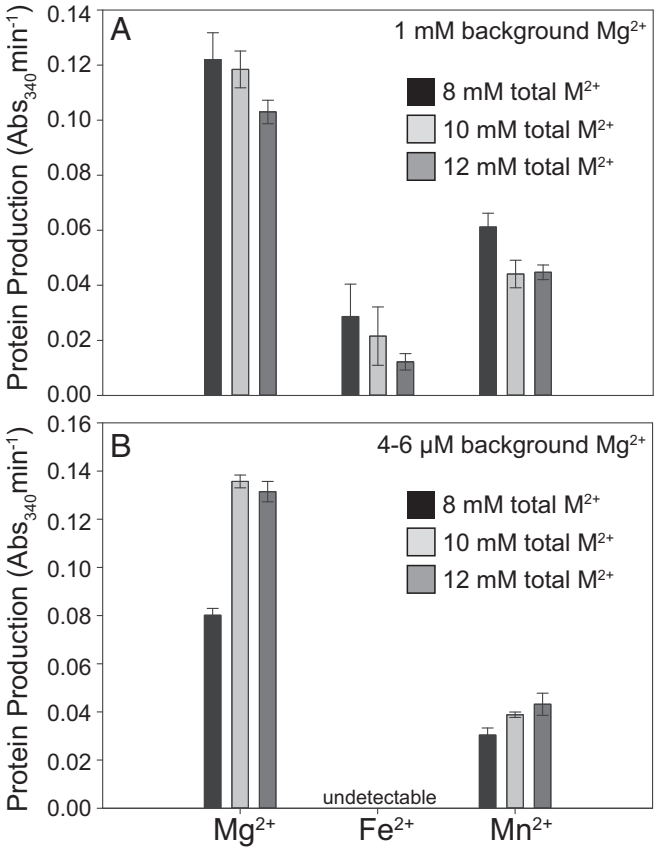


**Fig. 5.** $Mn^{2+}$ can support translation after removal of background $Mg^{2+}$. (*A*) Reactions prepared with washed *E. coli* ribosomes, reducing the background $Mg^{2+}$ to 1 mM, to which 7, 9, or 11 mM additional $Mg^{2+}$, $Fe^{2+}$, or $Mn^{2+}$ were added, totaling 8, 10, or 12 mM divalent cation ($M^{2+}$). (*B*) Reactions prepared using washed *E. coli* ribosomes and washed factor mix, which reduced the background $Mg^{2+}$ to the low-micromolar level, to which 8, 10, or 12 mM additional, $Mg^{2+}$, $Fe^{2+}$, or $Mn^{2+}$ were added. The activity of the translation product (DHFR, which catalyzes the oxidation of NADPH, with a maximum absorbance at 340 nm) was used as a proxy for protein production. The error bars for triplicate experiments ($n$ = 3) are plotted as the SEM.

of the remainder of the RNA polymer, and hydrogen atoms were added, where appropriate (*SI Appendix*, Fig. S4). Additional details on calculations adapted from previous publications (12, 22) are described in *SI Appendix*.

**ACKNOWLEDGMENTS.** We acknowledge helpful discussions with Corinna Tuckey (New England Biolabs) and with Eric B. O'Neill and Claudia Montllor Albalate (Georgia Institute of Technology). We thank Chieri Ito for technical assistance. We thank Michael Goodisman for access to a capillary electrophoresis instrument. This research was supported by the National Aeronautics and Space Administration Grants NNX14AJ87G, NNX16AJ28G, and NNX16AJ29G. The TXRF instrument was purchased and supported through the Georgia Institute of Technology School of Chemistry and Biochemistry, National Science Foundation Grant MCB1552791, and National Institutes of Health Grant ES02566 (to A.R.R.).

1. Derry LA (2015) Causes and consequences of mid-Proterozoic anoxia. *Geophys Res Lett* 42:8538–8546.
2. Jones C, Nomosatryo S, Crowe SA, Bjerrum CJ, Canfield DE (2015) Iron oxides, divalent cations, silica, and the early earth phosphorus crisis. *Geology* 43:135–138.
3. Poulton SW, Canfield DE (2011) Ferruginous conditions: A dominant feature of the ocean through Earth's history. *Elements* 7:107–112.
4. Holland HD (1984) *The Chemical Evolution of the Atmosphere and Oceans* (Princeton Univ Press, Princeton).
5. Johnson JE, Webb SM, Ma C, Fischer WW (2016) Manganese mineralogy and diagenesis in the sedimentary rock record. *Geochim Cosmochim Acta* 173:210–231.
6. Ramakrishnan V (2002) Ribosome structure and the mechanism of translation. *Cell* 108:557–572.
7. Yonath A (2002) The search and its outcome: High-resolution structures of ribosomal particles from mesophilic, thermophilic, and halophilic bacteria at various functional states. *Annu Rev Biophys Biomol Struct* 31:257–273.
8. Fox GE (2010) Origin and evolution of the ribosome. *Cold Spring Harb Perspect Biol* 2: a003483.
9. Bernier CR, Petrov AS, Kovacs NA, Penev PI, Williams LD (2018) Translation: The universal structural core of life. *Mol Biol Evol* 35:2065–2076.
10. Klein DJ, Moore PB, Steitz TA (2004) The contribution of metal ions to the structural stability of the large ribosomal subunit. *RNA* 10:1366–1379.
11. Cusack S (1997) Aminoacyl-tRNA synthetases. *Curr Opin Struct Biol* 7:881–889.
12. Petrov AS, Bowman JC, Harvey SC, Williams LD (2011) Bidentate RNA-magnesium clamps: On the origin of the special role of magnesium in RNA folding. *RNA* 17: 291–297.
13. Hsiao C, Williams LD (2009) A recurrent magnesium-binding motif provides a framework for the ribosomal peptidyl transferase center. *Nucleic Acids Res* 37: 3134–3142.
14. Schuwirth BS, et al. (2005) Structures of the bacterial ribosome at 3.5 Å resolution. *Science* 310:827–834.
15. Demeshkina N, Jenner L, Westhof E, Yusupov M, Yusupova G (2012) A new understanding of the decoding principle on the ribosome. *Nature* 484:256–259.
16. Selmer M, et al. (2006) Structure of the 70S ribosome complexed with mRNA and tRNA. *Science* 313:1935–1942.
17. Petrov AS, et al. (2012) RNA-magnesium-protein interactions in large ribosomal subunit. *J Phys Chem B* 116:8113–8120.
18. Pyle AM (2002) Metal ions in the structure and function of RNA. *J Biol Inorg Chem* 7: 679–690.
19. Pyle AM (1993) Ribozymes: A distinct class of metalloenzymes. *Science* 261:709–714.
20. Ward WL, Plakos K, DeRose VJ (2014) Nucleic acid catalysis: Metals, nucleobases, and other cofactors. *Chem Rev* 114:4318–4342.
21. Okafor CD, Bowman JC, Hud NV, Glass JB, Williams LD (2018) *Folding and Catalysis Near Life's Origin: Support for Fe2+ as a Dominant Divalent Cation. Prebiotic Chemistry and Chemical Evolution of Nucleic Acids* (Springer, New York), pp 227–243.
22. Athavale SS, et al. (2012) RNA folding and catalysis mediated by iron (II). *PLoS One* 7: e38024.
23. Popović M, Fliss PS, Ditzler MA (2015) *In vitro* evolution of distinct self-cleaving ribozymes in diverse environments. *Nucleic Acids Res* 43:7070–7082.
24. Okafor CD, et al. (2017) Iron mediates catalysis of nucleic acid processing enzymes: Support for Fe(II) as a cofactor before the great oxidation event. *Nucleic Acids Res* 45: 3634–3642.
25. Tabor S, Richardson CC (1989) Effect of manganese ions on the incorporation of dideoxynucleotides by bacteriophage T7 DNA polymerase and *Escherichia coli* DNA polymerase I. *Proc Natl Acad Sci USA* 86:4076–4080.
26. Litman RM (1971) The differential effect of magnesium and manganese ions on the synthesis of poly (dGd.C) and *Micrococcus luteus* DNA by *Micrococcus luteus* DNA polymerase. *J Mol Biol* 61:1–23.
27. Dann CE, 3rd, et al. (2007) Structure and mechanism of a metal-sensing regulatory RNA. *Cell* 130:878–892.
28. Mortimer SA, Weeks KM (2007) A fast-acting reagent for accurate analysis of RNA secondary and tertiary structure by SHAPE chemistry. *J Am Chem Soc* 129:4144–4145.
29. Athavale SS, et al. (2012) Domain III of the *T. thermophilus* 23S rRNA folds independently to a near-native state. *RNA* 18:752–758.
30. Hsiao C, et al. (2013) Molecular paleontology: A biochemical model of the ancestral ribosome. *Nucleic Acids Res* 41:3373–3385.
31. Lanier KA, Athavale SS, Petrov AS, Wartell R, Williams LD (2016) Imprint of ancient evolution on rRNA folding. *Biochemistry* 55:4603–4613.
32. Wilkinson KA, Merino EJ, Weeks KM (2006) Selective 2′-hydroxyl acylation analyzed by primer extension (SHAPE): Quantitative RNA structure analysis at single nucleotide resolution. *Nat Protoc* 1:1610–1616.
33. Lenz TK, Norris AM, Hud NV, Williams LD (2017) Protein-free ribosomal RNA folds to a near-native state in the presence of $Mg^{2+}$. *RSC Adv* 7:54674–54681.
34. Kigawa T, et al. (1999) Cell-free production and stable-isotope labeling of milligram quantities of proteins. *FEBS Lett* 442:15–19.
35. Goldberg A (1966) Magnesium binding by *Escherichia coli* ribosomes. *J Mol Biol* 15: 663–673.
36. Pronczuk AW, Baliga BS, Munro HN (1968) Effect of nucleoside triphosphate and magnesium ion concentration on the stability and function of rat liver polysomes *in vitro*. *Biochem J* 110:783–788.
37. Brion P, Westhof E (1997) Hierarchy and dynamics of RNA folding. *Annu Rev Biophys Biomol Struct* 26:113–137.
38. Tinoco I, Jr, Bustamante C (1999) How RNA folds. *J Mol Biol* 293:271–281.
39. Bock CW, Katz AK, Markham GD, Glusker JP (1999) Manganese as a replacement for magnesium and zinc: Functional comparison of the divalent ions. *J Am Chem Soc* 121: 7360–7372.
40. Imlay JA (2014) The mismetallation of enzymes during oxidative stress. *J Biol Chem* 289:28121–28128.
41. Zheng H, Shabalin IG, Handing KB, Bujnicki JM, Minor W (2015) Magnesium-binding architectures in RNA crystal structures: Validation, binding preferences, classification and motif detection. *Nucleic Acids Res* 43:3789–3801.
42. Bowman JC, Lenz TK, Hud NV, Williams LD (2012) Cations in charge: Magnesium ions in RNA folding and catalysis. *Curr Opin Struct Biol* 22:262–272.
43. Hensley MP, Tierney DL, Crowder MW (2011) Zn(II) binding to *Escherichia coli* 70S ribosomes. *Biochemistry* 50:9937–9939.
44. Craine JE, Peterkofsky A (1976) Studies on arginyl-tRNA synthetase from *Escherichia coli* B. Dual role of metals in enzyme catalysis. *J Biol Chem* 251:241–246.
45. Ito Y, Tomasselli AG, Noda LH (1980) ATP:AMP phosphotransferase from baker's yeast. Purification and properties. *Eur J Biochem* 105:85–92.
46. Da Silva JF, Williams RJP (2001) *The Biological Chemistry of the Elements: The Inorganic Chemistry of Life* (Oxford Univ Press, Oxford), 2nd Ed.
47. Daly MJ, et al. (2004) Accumulation of Mn(II) in *Deinococcus radiodurans* facilitates gamma-radiation resistance. *Science* 306:1025–1028.
48. Outten CE, O'Halloran TV (2001) Femtomolar sensitivity of metalloregulatory proteins controlling zinc homeostasis. *Science* 292:2488–2492.
49. Beauchene NA, et al. (2017) $O_2$ availability impacts iron homeostasis in *Escherichia coli*. *Proc Natl Acad Sci USA* 114:12261–12266.
50. Honda K, et al. (2005) Ribosomal RNA in Alzheimer disease is oxidized by bound redox-active iron. *J Biol Chem* 280:20978–20986.
51. Zinskie JA, et al. (2018) Iron-dependent cleavage of ribosomal RNA during oxidative stress in the yeast *Saccharomyces cerevisiae*. *J Biol Chem* 293:14237–14248.
52. Holmstrom ED, Fiore JL, Nesbitt DJ (2012) Thermodynamic origins of monovalent facilitated RNA folding. *Biochemistry* 51:3732–3743.
53. Ban N, Nissen P, Hansen J, Moore PB, Steitz TA (2000) The complete atomic structure of the large ribosomal subunit at 2.4 Å resolution. *Science* 289:905–920.
54. Bernier CR, et al. (2014) RiboVision suite for visualization and analysis of ribosomes. *Faraday Discuss* 169:195–207.
55. Keedy HE, Thomas EN, Zaher HS (2018) Decoding on the ribosome depends on the structure of the mRNA phosphodiester backbone. *Proc Natl Acad Sci USA* 115: E6731–E6740.
56. Kjeldgaard M, Nissen P, Thirup S, Nyborg J (1993) The crystal structure of elongation factor EF-Tu from *Thermus aquaticus* in the GTP conformation. *Structure* 1:35–50.
57. Campuzano S, Modolell J (1981) Effects of antibiotics, N-acetylaminoacyl-tRNA and other agents on the elongation-factor-Tu dependent and ribosome-dependent GTP hydrolysis promoted by 2′(3′)-O-L-phenylalanyladenosine. *Eur J Biochem* 117:27–31.
58. Chen Y, Feng S, Kumar V, Ero R, Gao Y-G (2013) Structure of EF-G-ribosome complex in a pretranslocation state. *Nat Struct Mol Biol* 20:1077–1084.
59. Lövgren TNE, Petersson A, Loftfield RB (1978) The mechanism of aminoacylation of transfer ribonucleic acid. The role of magnesium and spermine in the synthesis of isoleucyl-tRNA. *J Biol Chem* 253:6702–6710.
60. Thiebe R (1975) Aminoacylation of tRNA. Magnesium requirement and spermidine effect. *FEBS Lett* 51:259–261.
61. Blanquet S, Dessen P, Kahn D (1984) Properties and specificity of methionyl-tRNAfMet formyltransferase from *Escherichia coli*. *Methods Enzymol* 106:141–152.
62. Morin LG (1977) Creatine kinase: Stability, inactivation, reactivation. *Clin Chem* 23: 646–652.
63. Vasavada KV, Kaplan JI, Nageswara Rao BD (1984) Analysis of 31P NMR spectra of enzyme-bound reactants and products of adenylate kinase using density matrix theory of chemical exchange. *Biochemistry* 23:961–968.
64. Muñoz-Dorado J, Inouye S, Inouye M (1990) Nucleoside diphosphate kinase from *Myxococcus xanthus*. II. Biochemical characterization. *J Biol Chem* 265:2707–2712.
65. Kankare J, et al. (1994) The structure of *E. coli* soluble inorganic pyrophosphatase at 2.7 Å resolution. *Protein Eng Des Sel* 7:823–830, and erratum (1994) 7:1173.
66. Bloch-Frankenthal L (1954) The role of magnesium in the hydrolysis of sodium pyrophosphate by inorganic pyrophosphatase. *Biochem J* 57:87–92.